Available online at www.sciencedirect.com
ScienceDirect
Trans. Nonferrous Met. Soc. China 31(2021) 609−625
Transactions of Nonferrous Metals Society of China
www.tnmsc.cn

Microstructure and mechanical properties of 7005 aluminum alloy processed by one-pass equal channel reciprocating extrusion

Ju-fu JIANG[1], Ying WANG[2], Ying-ze LIU[1], Guan-fei XIAO[1], Hua LI[2]

1. School of Materials Science and Engineering, Harbin Institute of Technology, Harbin 150001, China;
2. School of Mechatronics Engineering, Harbin Institute of Technology, Harbin 150001, China

Received 12 April 2020; accepted 19 October 2020

Abstract: An equal channel reciprocating extrusion (ECRE) was proposed first to obtain a severe plastic deformation (SPD) of 7005 alloy. The microstructure and mechanical properties of one-pass ECREed (ECRE processed) 7005 alloy were investigated. The results show that SPD occurring in ECRE leads to a mixed microstructure. ECREed 7005 alloy exhibits a significant improvement of ultimate tensile strength (UTS) and elongation. Mechanical properties in the region undergoing a complete ECRE process are higher than those in the region undergoing an incomplete ECRE process due to larger dislocation strengthening effect. Yield strength (YS) and UTS first decrease and then increase with an increase of extrusion temperature. The YS of 359.2 MPa, UTS of 490 MPa and elongation of 17.7% are obtained after T6 treatment. Fine-grain strengthening, dislocation strengthening and precipitation strengthening in the T6-treated ECREed sample all play important roles in improving the mechanical properties.
Key words: 7005 aluminum alloy; equal channel reciprocating extrusion; microstructure; mechanical properties

1 Introduction

As a typical method to obtain nanometer or submicron grain-sized materials, equal channel angular extrusion (ECAE) or equal channel angular pressing (ECAP) has exhibited wide applications in aluminum alloys [1−5], magnesium alloys [6−8], copper alloys [9,10], titanium alloys [11,12], zinc alloys [13] and metal matrix composites [14,15]. Aluminum alloys have been the hottest materials among these metal materials since a large amount of research on ECAE or ECAP has been focused on the aluminum alloys. ECAP was applied to 1050 aluminum alloy [16], 7075 aluminum alloy [17], 5083 aluminum alloy [18], 7055 aluminum alloy [19] and Al−5wt.%Fe aluminum alloy [20] to obtain a strong refinement of microstructure and an significant improvement of mechanical properties. Besides hot extrusion, hot rolling and hot forging, ECAE was also a good strain-induced technology due to severe plastic deformation (SPD) obtained via shear deformation [21−23].

Actually, ECAE was not only used as a technology to obtain ultra-fine grained material, but also employed to obtain a good strain-induced effect for a fabrication of semisolid slurry of magnesium alloy [24−26]. Applications of ECAE to magnesium alloys have exhibited the feasibility of ECAE as a strain-induced method [27−30]. Besides magnesium alloys, ECAE also showed an effective severe plastic deformation on the aluminum alloys [31−34].

However, the good strain-induced effect was obtained after at least two-pass ECAE (or ECAP) was carried out on magnesium alloys and aluminum alloys. This indicates that multi-pass ECAE process had to be performed to obtain a good strain-induced effect. As a consequence, it increases the operating difficulties in performing the second extrusion and

Corresponding author: Ying WANG; Tel: +86-15945697615; E-mail: wangying1002@hit.edu.cn
DOI: 10.1016/S1003-6326(21)65523-1

the production cost of the semisolid slurry. SPUSKANYUK et al [35] developed double-angle equal-channel angular hydroextrusion (ECAH) to solve the above-mentioned difficulty. In their research, the intersecting angle of two channels (Φ) was 120°, the angle subtended by the arc of curvature at the point of intersection (Ψ) was 0° and the diameter of the channel was 16 mm.

In the present research, we develop a novel technology called equal channel reciprocating extrusion (ECRE) to realize a severe plastic deformation via only one pass. The differences between ECAH and ECRE are the intersecting angle of two channels, the angle subtended by the arc of curvature at the point of intersection and the diameter of two channels. Research on SPD of 7005 aluminum alloy was reported little. Therefore, a new SPD method will be applied to this material in the present research. Two-pass ECAE was realized only via one ECRE process. It will avoid the second extrusion during ECAE process, and decrease the cost in fabricating fine-grain material. In addition, a larger deformation degree can be obtained via ECRE as compared to conventional open blank forging. To evaluate the effect of one-pass ECRE on 7005 alloy, we examine the microstructure and mechanical properties of material processed by one-pass ECRE.

2 Experimental

The 7005 commercial alloy was used as experimental material. Its chemical composition was measured via a PANalytical PW4400 X-ray fluorescence spectrometer to contain 5.1Zn, 1.1 Mg, 0.49 Mn, 0.34 Si, 0.31 Fe, 0.1 Cr, 0.08 Cu, 0.04 Ti and balanced Al (in wt.%). 7005 alloy was firstly melted at 660 °C and then poured into a cylinder cast ingot with a diameter of 58 mm. The cast ingots were machined into cylindrical samples with a diameter of 54.6 mm and a height of 100 mm. A set of ECRE die with 55 mm in inner diameter of two sectional female dies was designed and manufactured, as shown in Fig. 1(a). The intersecting angle between two equal cross-sectional channels (Φ) was 90°. Two sectional female dies

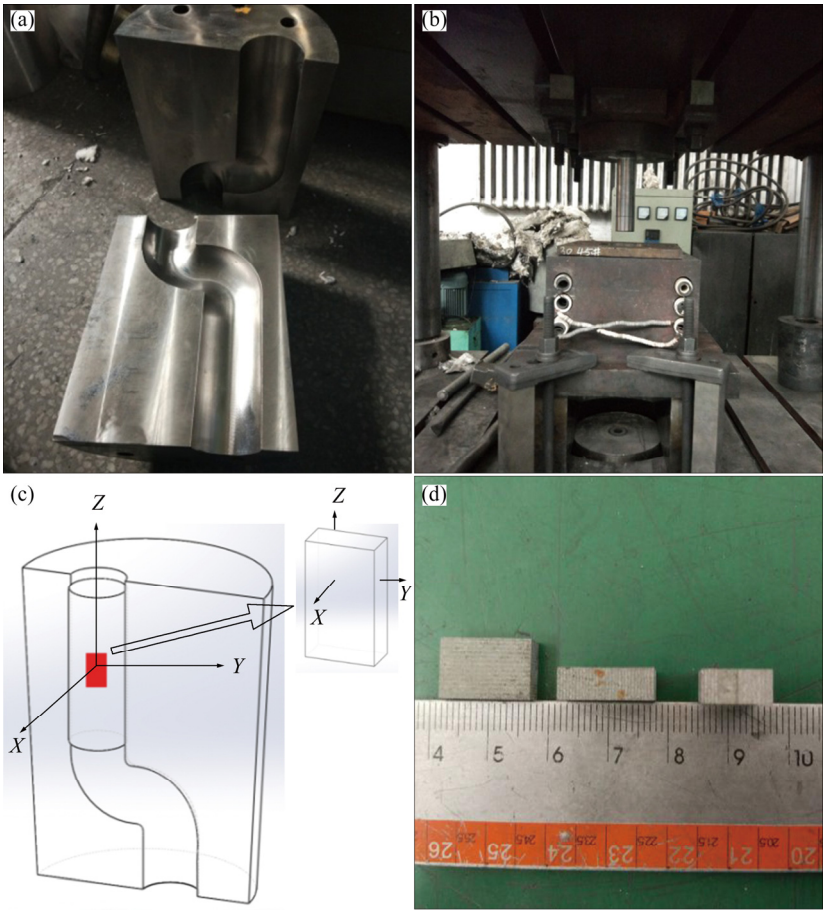

Fig. 1 Macrographs of two half-sectional dies (a) and whole die (b), schematic diagram of coordinate system (c), and microstructural samples (d)

were put in a square die sleeve with a resistant heating device (Fig. 1(b)). The lubricant of water-based graphite was sprayed on the surface of the punch and the two sectional female die at 120 °C. This reduced an adverse effect of friction on ECRE process. The machined samples were heated to 360, 380, 400 and 420 °C, respectively, and then extruded for one pass via the ECRE die. The ECRE die was preheated to the same temperature with the heated samples. The previous sample was firstly extruded to a position of about 120 mm in distance from the top surface of the two sectional female dies. Then, the latter sample was put in the cavity which was composed of the two sectional female dies and then extruded. The rest samples were done repeatedly in the same manner. A rectangular coordinate system was established to describe the microstructure accurately in various coordinate planes (Fig. 1(c)). The macrograph of the cut specimens was presented in Fig. 1(d).

The microstructure and mechanical properties of cast ingots and ECREed 7005 alloy were examined (Fig. 2(a)). Figure 2(b) shows a drawing of tensile specimen according to the PRC National Standard GB 6397—86 [36]. The incompletely ECREed 7005 alloy billets were taken out from the die during the middle ECRE process. And the microstructure and mechanical properties of incompletely ECREed (ECRE processed) billet were examined. The microstructural specimens of incompletely ECREed 7005 alloy were cut from the Locations 1 and 2 of Billet 1 (B1) and Locations 3, 4 and 5 of Billet 2 (B2), as shown in Fig. 2(c). The tensile specimens of incompletely ECREed 7005 billet were cut from the Locations 6 and 7 (Fig. 2(d)).

The microstructural and tensile specimens of completely ECREed 7005 alloy were cut from the locations shown in Fig. 2(e). T6 heat treat involving 30 min solution treatment at 470 °C and 24 h artificial aging at 110 °C was conducted on the completely ECREed 7005 alloy and the mechanical properties of billet and those without T6 heat treatment were compared.

The tensile tests were carried out on the machined tensile samples by an AG-X Plus 250 kN universe material testing machine at a rate of 1 mm/min. The tensile fracture was observed via a Quanta 200FEG field emission scanning electron microscope (SEM). The microstructural specimens

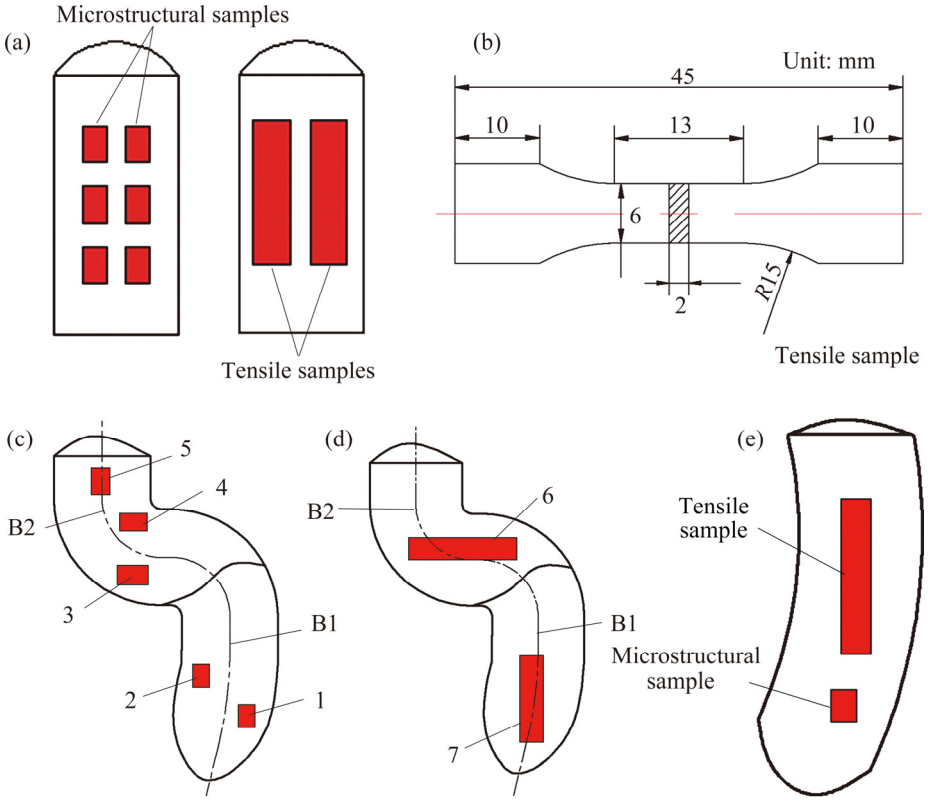

Fig. 2 Sampling locations of microstructure and tensile specimens of cast ingot (a), drawing of tensile specimen (b) and sampling locations of ECREed 7005 alloy (c−e)

cut from the ECREed 7005 alloy were ground with 200, 400, 600, 800, 1200 and 2000 grit papers and polished with 0.1 μm diamond paste. Some specimens were etched for about 10 s by Keller's reagent (4 mL HF, 6 mL HCl, 8 mL HNO_3 and 82 mL water) and used as metallographic observation samples via an Olympus GX71 optical microscope (OM). The other specimens were electrochemically polished with a mixed solution of perchloric acid and absolute ethyl alcohol (10 mL 70 vol.% $HClO_4$ and 90 mL C_2H_6O) and used as electron backscattered diffusion (EBSD) observation samples via a Quanta 200FEG field emission SEM with orientation analysis system. The voltage and current in electrochemical polishing were 20 V and 0.3 A, respectively. The time of electrochemical polishing was 35 s. A Talos F200x transmission electron microscopy (TEM) with an energy dispersive spectroscopy (EDS) was employed to characterize the microstructure of the ECREed 7005 alloy.

3 Results

3.1 Microstructure and mechanical properties of incompletely ECREed 7005 alloy

The microstructures and engineering stress−strain curves of 7005 alloy cast ingot are presented in Figs. 3 and 4, respectively. As shown in Fig. 3, obvious dendrite is found in the microstructure of 7005 alloy cast ingot. The grain size of the microstructure on *X* coordinate plane (i.e. longitudinal direction) is larger than 200 μm (Fig. 3(a)). The grain size of the microstructure on *Y* coordinate plane (i.e. the other longitudinal direction) is smaller than that on *X* coordinate plane (Fig. 3(b)). The grain size of the microstructure on the *Z* coordinate plane (i.e. transverse direction) is close to that on *X* coordinate plane (Fig. 3(c)). The dendrite morphology in three coordinate planes illustrates that the microstructure is characterized by a typical cast microstructure (i.e. dendrites). As shown in Fig. 4, the yield strength (YS) of (290.6±12.6) MPa, ultimate tensile strength (UTS) of (307.1±8.2) MPa and elongation of (0.75±0.13)% are obtained from the engineering stress−strain curve of cast ingot. The value of elongation is very small, indicating that a brittle fracture occurs during the tensile process of cast ingot.

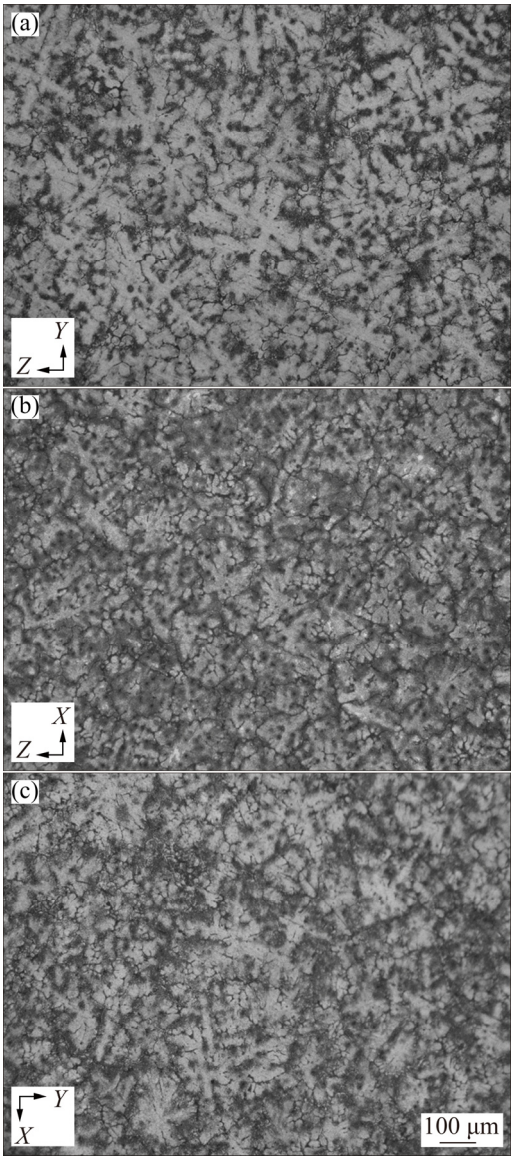

Fig. 3 Microstructures of cast ingot of 7005 aluminum alloy: (a) On *X* coordinate plane; (b) On *Y* coordinate plane; (c) On *Z* coordinate plane

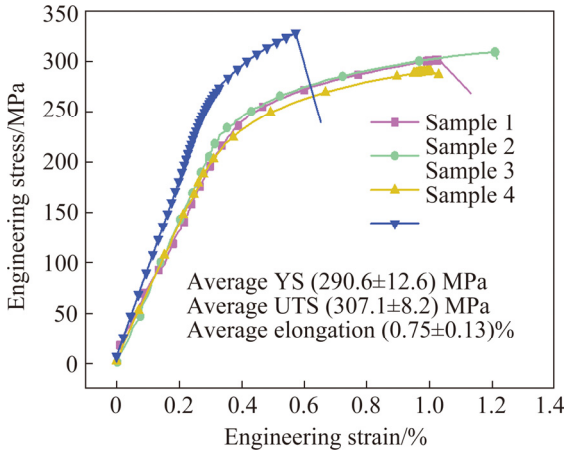

Fig. 4 Engineering stress−strain curves of cast ingot of 7005 aluminum alloy

The longitudinal microstructures (*X* coordinate plane) at various locations of 7005 alloy during the middle ECRE process are shown in Fig. 5. As shown in Fig. 5, the microstructure at Locations 1−5 consists of elongated grains, equiaxed grains and deformed dendrites. The size of the deformed dendrites in the microstructure of ECREed 7005 alloy is less than that of the dendrite in cast ingot. The grain sizes of the microstructure at Locations 3, 4 and 5 are larger than those at Locations 1 and 2. More equiaxed grains are found at Location 2 as compared with other locations. Figure 6 gives transverse microstructures (*Z* coordinate plane) at various locations during ECRE process of ECREed 7005 alloy. Similar to Figs. 5(a, b), the microstructures at Locations 1 and 2 consist of elongated grains, equiaxed grains and deformed dendrites. In addition, the grain size on *Z* coordinate plane is smaller than that on *X* coordinate plane. Figure 7 presents engineering stress−stress curves of ECREed 7005 alloy, and YS, UTS and elongation at Location 6 are 228.3 MPa, 430.9 MPa and 13.2%, respectively.

As shown in Fig. 7, YS, UTS and elongation at Location 7 are 226.3 MPa, 440.1 MPa and 18%, respectively. The YS at Locations 6 and 7 decreases as compared to that of cast ingot. However, the UTS and elongation at Locations 6 and 7 increase significantly compared to those of cast ingot. The UTS values at Locations 6 and 7 are increased by 40.3% and 43.3%, respectively. Especially, the elongation values at Locations 6 and 7 are 16.6 and 23.0 times higher than that of cast ingot. In addition, it can be noted that UTS and elongation at Location 7 are higher than those at Location 6.

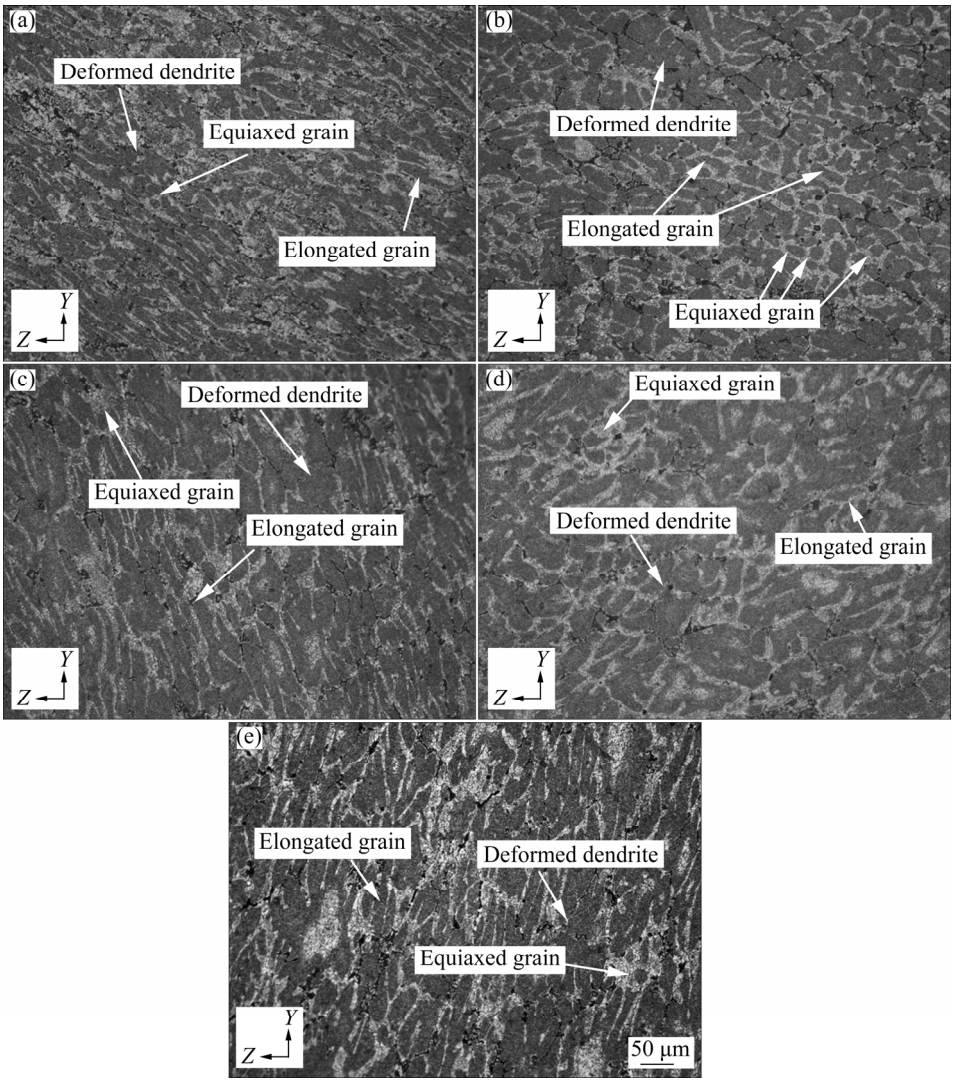

Fig. 5 Longitudinal microstructures (*X* coordinate plane) at various locations of 7005 alloy during middle ECRE process: (a) Location 1; (b) Location 2; (c) Location 3; (d) Location 4; (e) Location 5

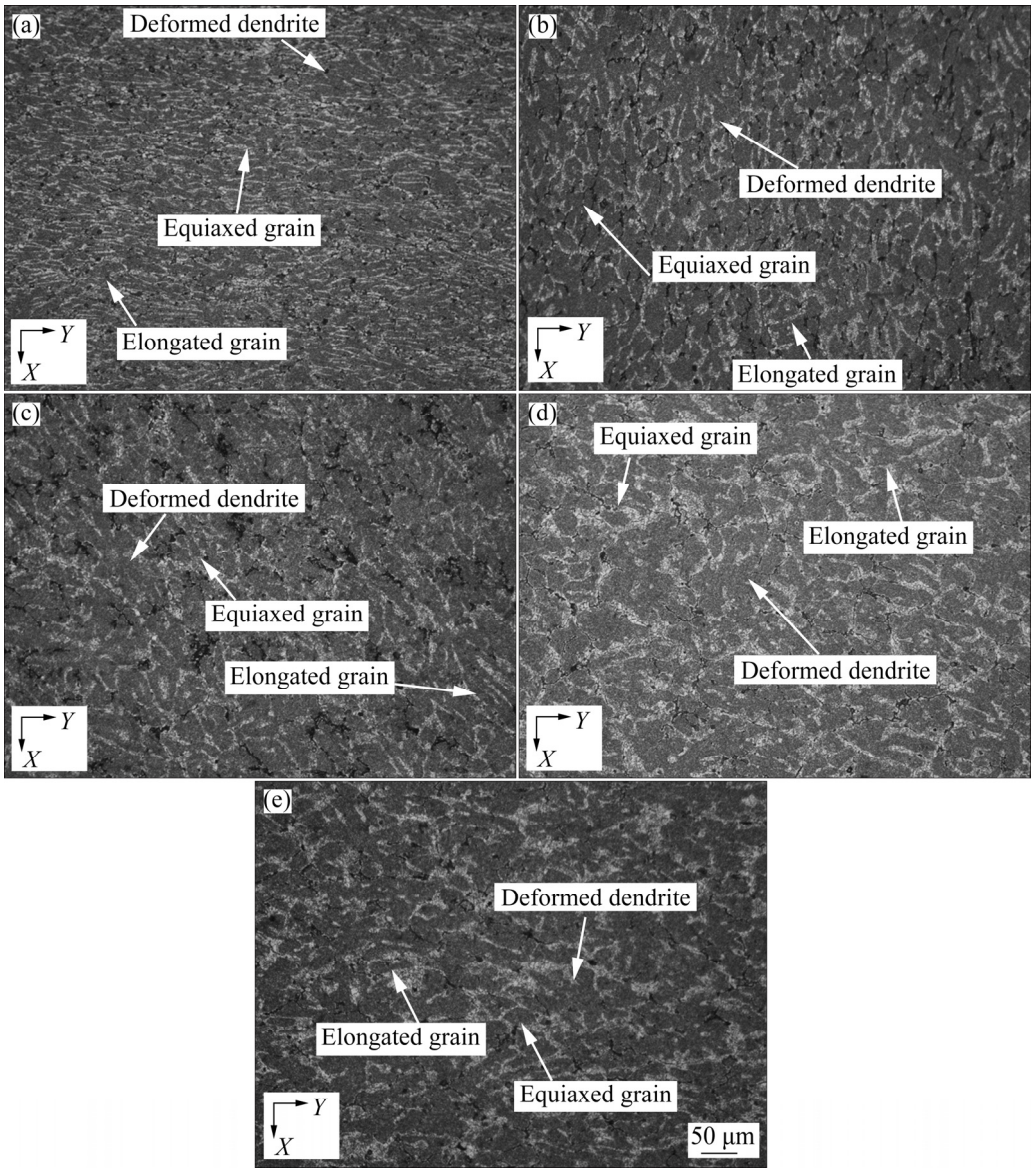

Fig. 6 Transverse microstructures (*Z* coordinate plane) at various locations of 7005 alloy during middle ECRE process: (a) Location 1; (b) Location 2; (c) Location 3; (d) Location 4; (e) Location 5

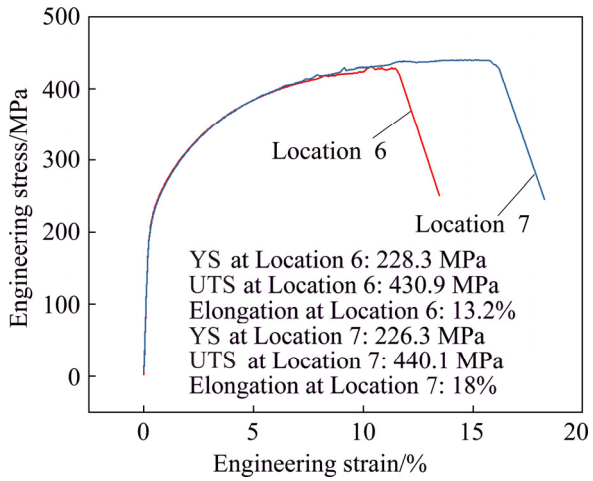

Fig. 7 Engineering stress−strain curves of ECREed 7005 alloy samples obtained from Locations 6 and 7

3.2 Effect of extrusion temperature on microstructure and mechanical properties of one-pass ECREed 7005 alloy

Figure 8 shows macrographs of one-pass ECREed 7005 alloy at different extrusion temperatures. It can be noted that the shape of the one-pass ECREed 7005 alloy is obviously changed. A cone shape is formed in the front zone after one-pass ECRE process. This is attributed to the effect of friction on ECRE process. The OM microstructures on *X* coordinate plane of ECREed 7005 alloy at various extrusion temperatures are presented in Fig. 9. As shown in Fig. 9, the microstructures consist of the elongated grains, equiaxed grains and deformed dendrite. The size of

Fig. 8 Macrographs of one-pass ECREed 7005 alloy at different extrusion temperatures

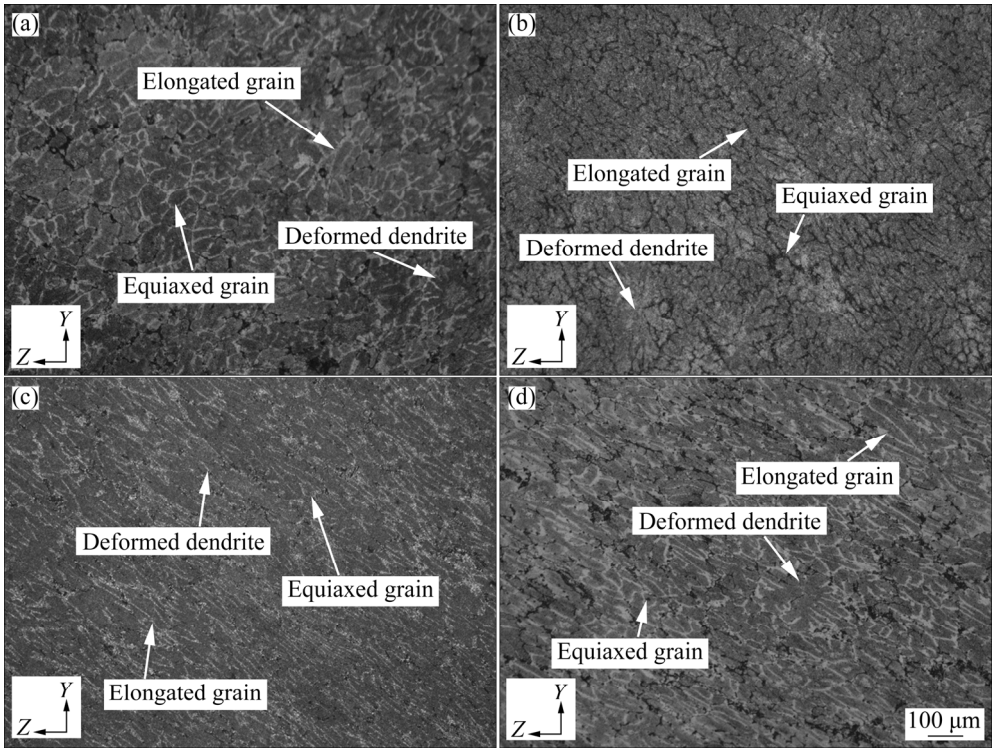

Fig. 9 Microstructures on *X* coordinate plane of ECREed 7005 alloy at various extrusion temperatures: (a) 360 °C; (b) 380 °C; (c) 400 °C; (d) 420 °C

the deformed dendrites is smaller than that of the dendrite in cast ingot. This is attributed to the effect of severe plastic deformation caused by ECRE process.

Figure 10 shows the microstructures on *Z* coordinate plane of ECREed 7005 alloy at different extrusion temperatures. Similar to Fig. 9, the transverse microstructure involves elongated grain, equiaxed grains and deformed dendrites. As indicated in Fig. 11, the YS and UTS show a decreased trend with an increase of extrusion temperature from 360 to 400 °C, but they increase again with an increase of extrusion temperature from 400 to 420 °C. The elongation exhibits a peak value at 400 °C. The highest YS of 288.9 MPa is obtained at 360 °C. The highest UTS of 441.2 MPa is achieved at 420 °C, and the highest elongation of 18.2% is obtained at 400 °C.

3.3 Effect of T6 treatment on microstructure and mechanical properties of one-pass ECREed 7005 alloy

Figure 12 shows the OM microstructures of cast ingot and one-pass ECREed 7005 alloy after T6 treatment. As shown in Fig. 12(a), the microstructure of cast ingot with T6 treatment consists

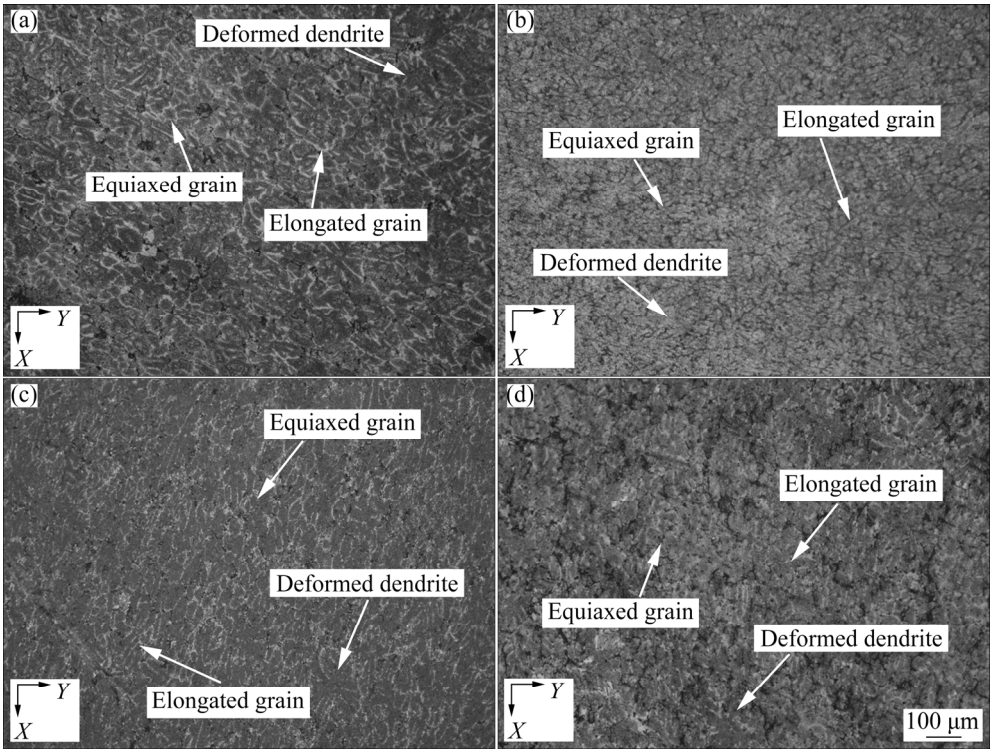

Fig. 10 Microstructures on *Z* coordinate plane of ECREed 7005 alloy at different extrusion temperatures: (a) 360 °C; (b) 380 °C; (c) 400 °C; (d) 420 °C

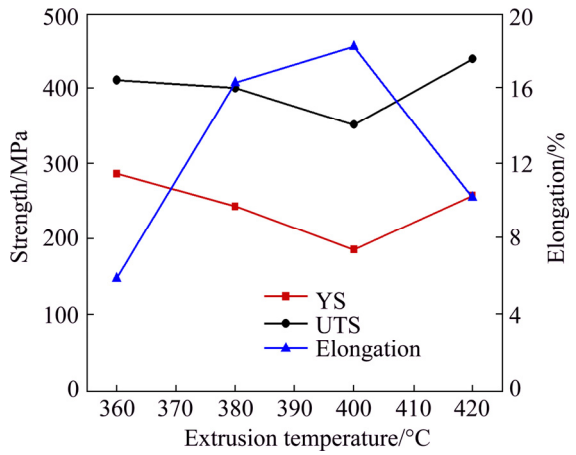

Fig. 11 Mechanical properties of one-pass ECREed 7005 alloy at different extrusion temperatures

of dendrites. Furthermore, it can be noticed that the size of dendrites is larger than that of cast ingot without T6 treatment (Fig. 3). The microstructure of ECREed billet consists of elongated grains, equiaxed grains and deformed dendrites (Fig. 12(b)). The sizes of elongated grains, equiaxed grains and deformed dendrites increase as compared with those of the billet without T6 treatment. This is attributed to grain growth caused by elevated temperature during the solution treatment. In addition, it can be noted that the grain boundary

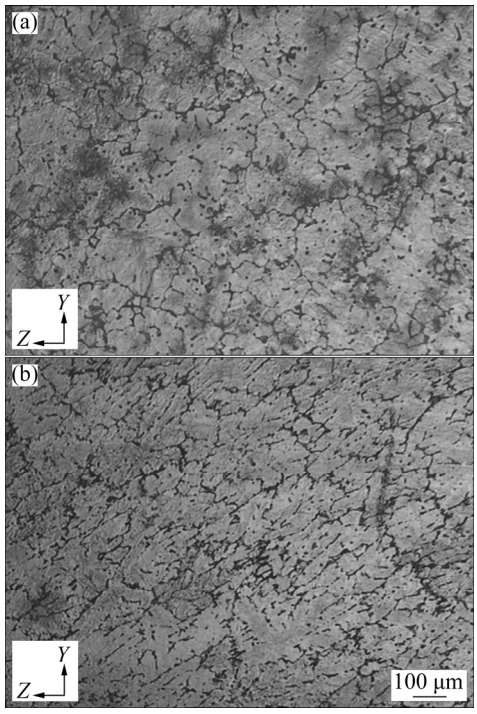

Fig. 12 Microstructures of cast ingot (a) and one-pass ECREed billet (b) of 7005 alloy after T6 treatment

of billet with T6 treatment becomes obscure as compared to that of billet without T6 treatment. It is due to the diffusion of alloying elements on the grain boundary.

As shown in Fig. 13, the mechanical properties of cast ingot and ECREed 7005 alloy billet are significantly improved as compared to those of the billet without T6 treatment. The YS, UTS and elongation of cast ingot with T6 treatment are 427.7 MPa, 455.6 MPa and 2.2%, respectively. The YS, UTS and elongation of ECREed 7005 alloy with T6 treatment are 359.2 MPa, 490 MPa and 17.7%, respectively. The YS, UTS and elongation of cast ingot with T6 treatment are increased by 30.6%, 38.8% and 495%, respectively, as compared to those of cast ingot without T6 treatment. The YS, UTS and elongation of ECREed 7005 alloy with T6 treatment are increased by 38%, 16.7% and 71.8%, respectively, as compared to those of ECREed 7005 alloy without T6 treatment. Similar to billet without T6 treatment, the YS of cast ingot with T6 treatment is higher than that of ECREed 7005 alloy billet with T6 treatment.

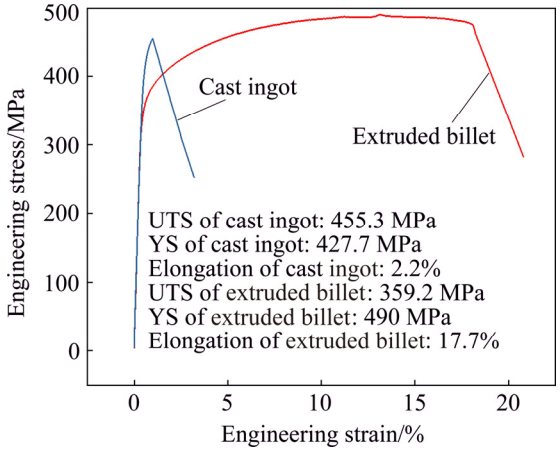

Fig. 13 Engineering stress−strain curves of cast ingot and ECREed billet of 7005 alloy

4 Discussion

As shown in Fig. 2, Locations 1 and 2 correspond to the Billet 1 that almost undergoes a complete ECRE (i.e. two ECAE processes). Location 3 corresponds to Billet 2, indicating a complete ECAE process. So, the plastic degree at Location 3 is less than that at Locations 1 and 2. The material at Location 4 is just in the process of ECAE, but the material at Location 5 does not undergo ECAE deformation. Therefore, the microstructures at Locations 4 and 5 possess large-size elongated grains and deformed dendrites (Fig. 5). Formation of equiaxed grains is attributed to severe plastic deformation and dynamic recrystallization occurring in the ECRE process. More equiaxed grains formed at Location 2 is due to larger plastic deformation as compared to other locations. A larger plastic deformation leads to more dislocation pile-up, which can accelerate the nucleation of dynamic recrystallization [37]. Dendrite arms at Locations 1−5 are deformed severely and more dislocations are created in the dendrites. These deformed dendrites with a large number of dislocations are beneficial to forming spheroidal grains during the semisolid isothermal treatment (SSIT) [38]. Furthermore, the plastic deformation degree of the deformed dendrite at Locations 3−5 is smaller than that at Locations 1 and 2 due to an incomplete ECRE deformation. A similar law is also noticed in the transverse microstructure due to different plastic deformation degrees (Fig. 6).

Figure 14 gives statistics results of equiaxed grains, deformed dendrite and elongated grains at each location. As shown in Fig. 14, the numbers of equiaxed grains at Locations 1−5 of the longitudinal microstructure (X coordinate plane) are 24, 44, 21, 26 and 13, respectively. This also illustrates quantitatively that the number of equiaxed grains at Location 2 of the longitudinal microstructure is much more than that at Locations 1, 3, 4 and 5. A similar law is found in the transverse microstructure (Z coordinate plane), as indicated in Fig. 14. This is attributed to larger plastic deformation occurring at Location 1 as compared to other locations.

As shown in Fig. 7, the YS at Location 7 is close to that at Location 6, but UTS and elongation at Location 7 are significantly higher than those at Location 6. In particular, the elongation at

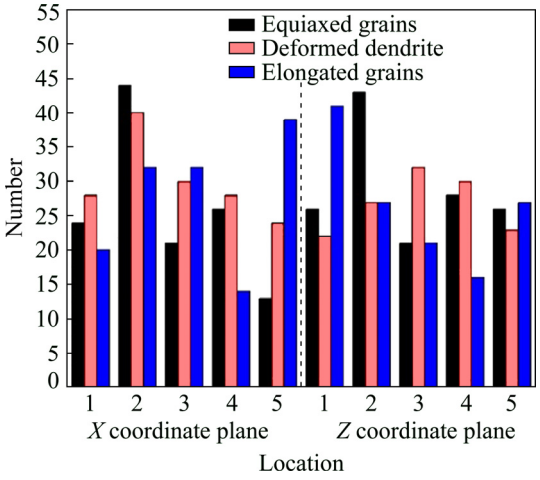

Fig. 14 Statistics results of equiaxed grains, deformed dendrite and elongated grains at each location

Location 7 is 36% higher than that at Location 6. This is attributed to larger plastic deformation at Location 7. The material at Location 6 only undergoes one ECAE process, but the material at Location 7 undergoes two ECAE processes (i.e. ECRE). The accumulative deformation in ECAE process can be calculated by [39]

$$\varepsilon=N\left[\frac{2\cot\left(\Phi/2+\Psi/2\right)+\Psi\operatorname{cosec}\left(\Phi/2+\Psi/2\right)}{\sqrt{3}}\right] \quad (1)$$

where ε is the accumulated deformation, N is the extrusion pass, Φ is the intersecting angle between two equal cross-sectional channels and Ψ is the angle subtended by the arc of curvature at the point of intersection. Here, the Φ and Ψ are all $\pi/2$. Hence, Eq. (1) can be transformed into [7]:

$$\varepsilon=0.9N \quad (2)$$

A complete ECRE process corresponds to two complete ECAE processes. Therefore, the accumulative deformation of a complete ECRE process can be derived from the accumulative deformation formula of ECAE (i.e. Eqs. (1) and (2)). The accumulative deformation of a complete ECRE process can be described as

$$\varepsilon=1.8N \quad (3)$$

Here, N is 1, so the accumulative deformation of a complete ECRE process is 1.8. The total deformation at Location 7 (i.e. equivalent strain of 3.6) is double that at Location 6. The deformation at Location 7 is obviously larger than that at Location 6. Therefore, larger working hardening at Location 7 leads to an improvement of mechanical properties at Location 7 as compared with those at Location 6.

Figure 15 shows EBSD results at various locations of 7005 alloy during the middle ECRE process. There are three kinds of typical micro-structure: deformed structure (i.e. grain orientation spread (GOS) more than 3.0°), substructure (i.e. GOS between 1.8° and 3°) and recrystallized structure (i.e. GOS less than 1.8°) in the 7005 alloy during ECRE process. The fractions of deformed

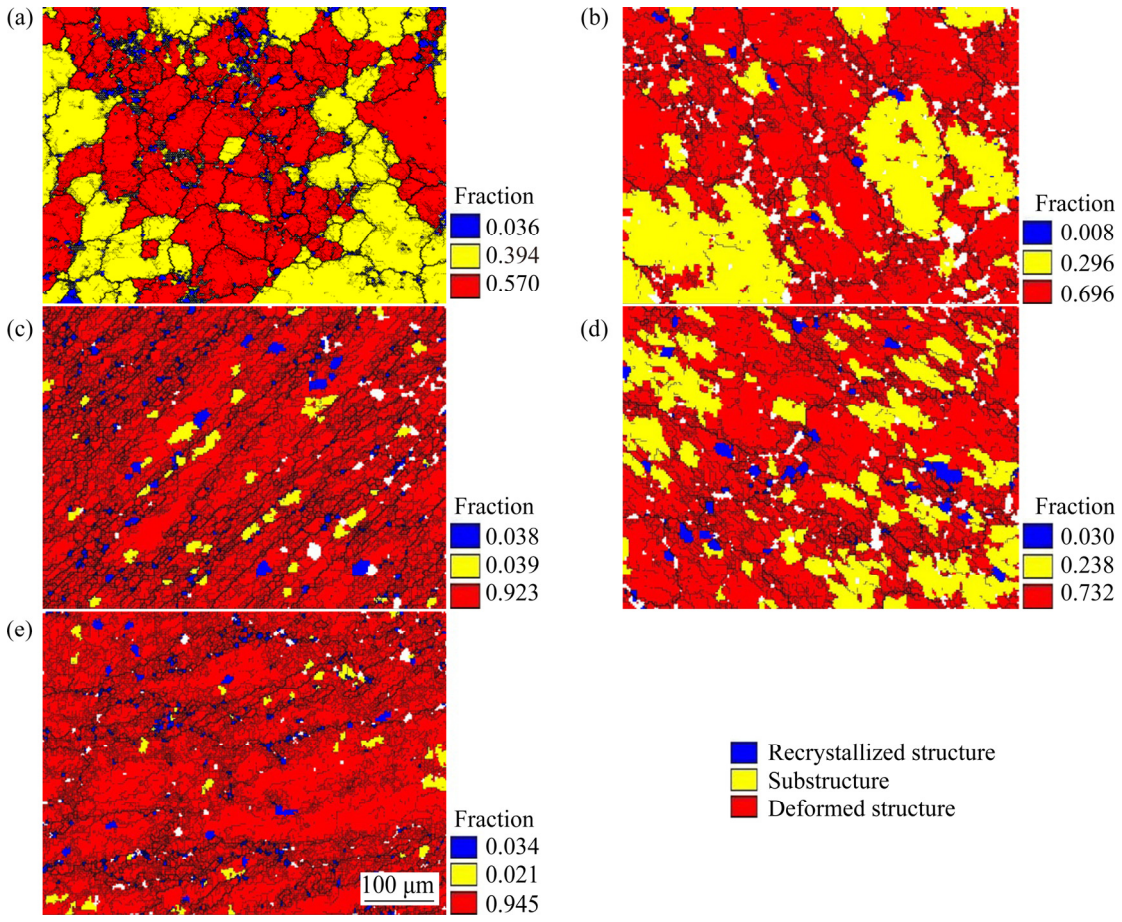

Fig. 15 EBSD results at various locations of 7005 alloy during middle ECRE process: (a) Location 5; (b) Location 4; (c) Location 3; (d) Location 2; (e) Location 1

structure, substructure and recrystallized structure at Location 5 are 0.570, 0.394 and 0.036, respectively (Fig. 15(a)). The fractions of deformed structure, substructure and recrystallized structure at Location 4 are 0.696, 0.296 and 0.008, respectively (Fig. 15(b)). This illustrates that only a small amount of dynamic recrystallization occurs during the ECRE process. A large amount of low angle grain boundary is formed due to SPD. With an increase of deformation degree, SPD is still the main deformation mechanism (Figs. 15(c−e)).

The fractions of the substructure at Locations 5, 4 and 2 are larger than those at Locations 1 and 3. This indicates that more subgrains with GOS of 1.8°−3° are formed at Locations 5, 2 and 4. Fraction of recrystallized structure at Locations 1, 2, 3 and 5 increases as compared with that at Location 4 (Fig. 15). This indicates that more recrystallized grains are formed at these locations during the ECRE process. To sum up, deformed structure occupies the largest area at these locations, implying that severe plastic deformation occurs during ECRE process. This illustrates that the working hardening (i.e. dislocation strengthening mechanism) plays an important role in improving the mechanical properties of one-pass ECREed 7005 alloy.

In addition, high density dislocations are noticed at Locations 6 and 7 (Fig. 16). As indicated in Fig. 16(a), dislocation and dislocation wall are found in the TEM image at Location 6. An obvious dislocation net is noticed in the TEM microstructure at Location 7 (Fig. 16(b)). This illustrates that the dislocation density at Location 7 is higher as compared to that at Location 6. This further confirms that larger plastic deformation occurs at Location 7. As a consequence, the mechanical properties of material at Location 7 are improved due to higher dislocation density. Figure 17 also gives a confirmation of the enhancement of UTS and elongation of ECREed 7005 alloy as compared to cast ingot. As shown in Fig. 17(a), an obvious cleavage is found in the fracture microstructure of cast ingot, indicating brittle fracture. In addition, a crack is noticed in the fracture microstructure of cast ingot. This also illustrates that the UTS and elongation of cast ingot decrease significantly. A large number of small-size dimples are created in the fracture microstructure of ECREed 7005 alloy (Figs. 17(b, c)). This indicates that the fracture of ECREed 7005 alloy is characterized by ductile fracture, leading to an improvement of UTS and elongation.

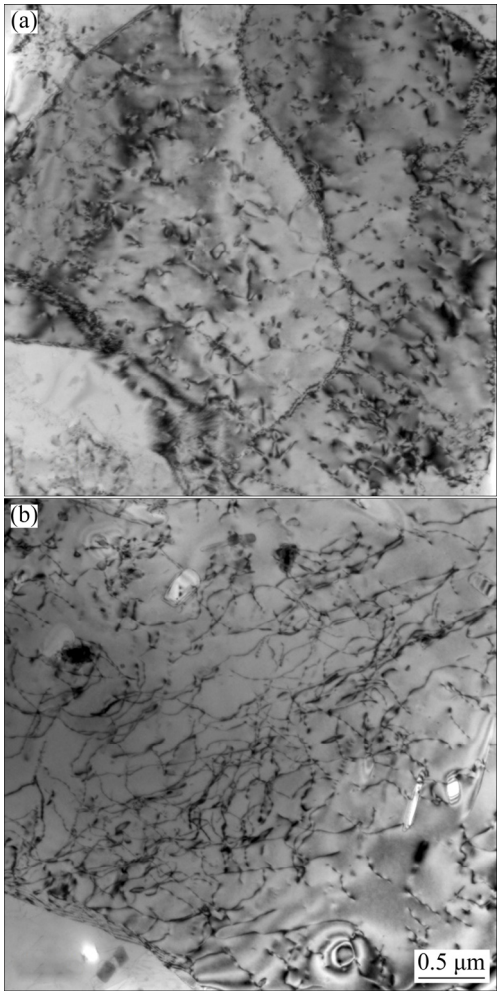

Fig. 16 TEM images at different locations of 7005 alloy during middle ECRE process: (a) Location 6; (b) Location 7

Friction has an important influence on the flowing behavior of the material during ECRE process. This leads to inhomogeneous plastic deformation during the ECRE process (Fig. 8). The flow velocity of the middle part of the ECREed material is larger than that of the peripheral part contacting the die due to smaller friction force. If the sectional dimension of the processed billet is less than 10 mm, the effect of shape change of the processed billet is little [1,3]. However, in this research, the sectional dimension is increased to 55 mm, and the effect of friction is more dominant, leading to a cone shape after one-pass ECRE. The AZ61 magnesium alloy with a large section size also exhibited an obvious shape change [7]. The

microstructure of one-pass ECREed 7005 alloy at various extrusion temperatures is deformed significantly as compared to that of cast ingot (Fig. 9 and 10). The dendrite arms are elongated along the flowing direction of material. Some second dendrite arms are separated from the primary dendrites to form some fine equiaxed grains due to dynamic recrystallization.

Figure 18 shows the TEM images of one-pass ECREed 7005 alloy at various extrusion temperatures. When the extrusion temperature is 360 °C, an obvious dislocation tangle is found in the TEM image. This indicates a large dislocation density at 360 °C (Fig. 18(a)). When extrusion temperature reaches 380 °C, dislocation density decreases slightly as compared to that at 360 °C. Some dislocations move regularly to form the dislocation walls, leading to a slight decrease of dislocation density (Fig. 18(b)). In addition, new grain boundary with little dislocation is found in the

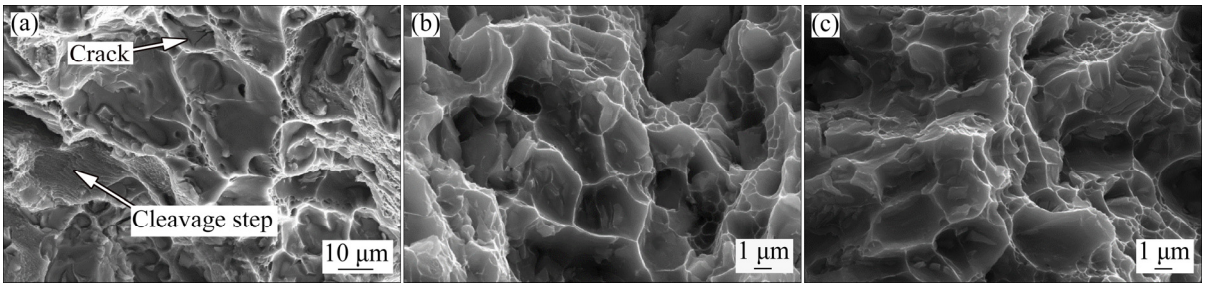

Fig. 17 Tensile fracture morphologies of cast ingot (a) and ECREed 7005 alloy at Location 6 (b), and Location 7 (c)

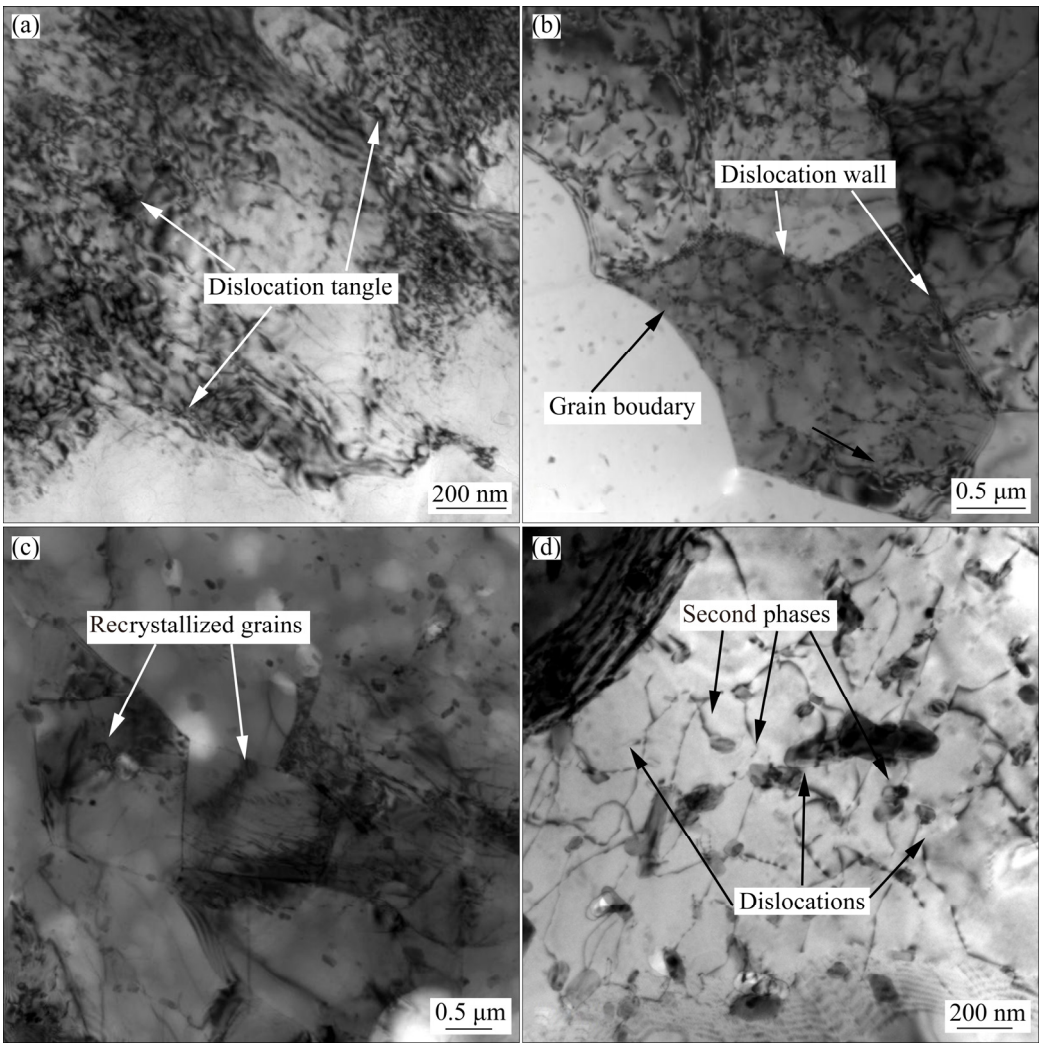

Fig. 18 TEM images of one-pass ECREed 7005 alloy at various extrusion temperatures: (a) 360 °C; (b) 380 °C; (c) 400 °C; (d) 420 °C

TEM image. This illustrates that the dislocation density is decreased at elevated extrusion temperature, attributed to the dynamic recovery occurring in ECRE process. As a result, the YS and UTS of ECREed 7005 alloy at 380 °C decrease and the elongation increases (Fig. 11). Some recrystallized grains are found in the microstructure. This indicates that the dislocation density is further decreased with an increase of extrusion temperature (Fig. 18(c)).

There are still some dislocations in the recrystallized grains. A similar phenomenon was also found in the TEM image of pure aluminum processed by ECAP-Conform technology [40]. A further decrease of YS and UTS and an increase of elongation occur at 400 °C (Fig. 11). However, some obvious second phase and dislocations exist together in the microstructure (Fig. 18(d)). The second phase has an elliptical shape or strip shape. The size of the elliptical second phase is about 100 nm. The length of the strip second phase varies from 150 to 300 nm. The formation of the second phase may be due to the natural aging after ECRE process. When 7005 alloy is deformed during ECRE process, the severe deformation in ECRE also enhances the precipitation of the second phase during the following natural aging. Furthermore, the interaction between the second phase and dislocation is noticed in the TEM image. The second phase hinders the motivation of the dislocation during the deformation. In order to make the dislocations move further, a larger force must be applied. It could be the reason that the YS and UTS increase again when the extrusion temperature is increased from 400 to 420 °C (Fig. 11).

Figure 19 shows the pole figure of ECREed 7005 alloy at various extrusion temperatures. As

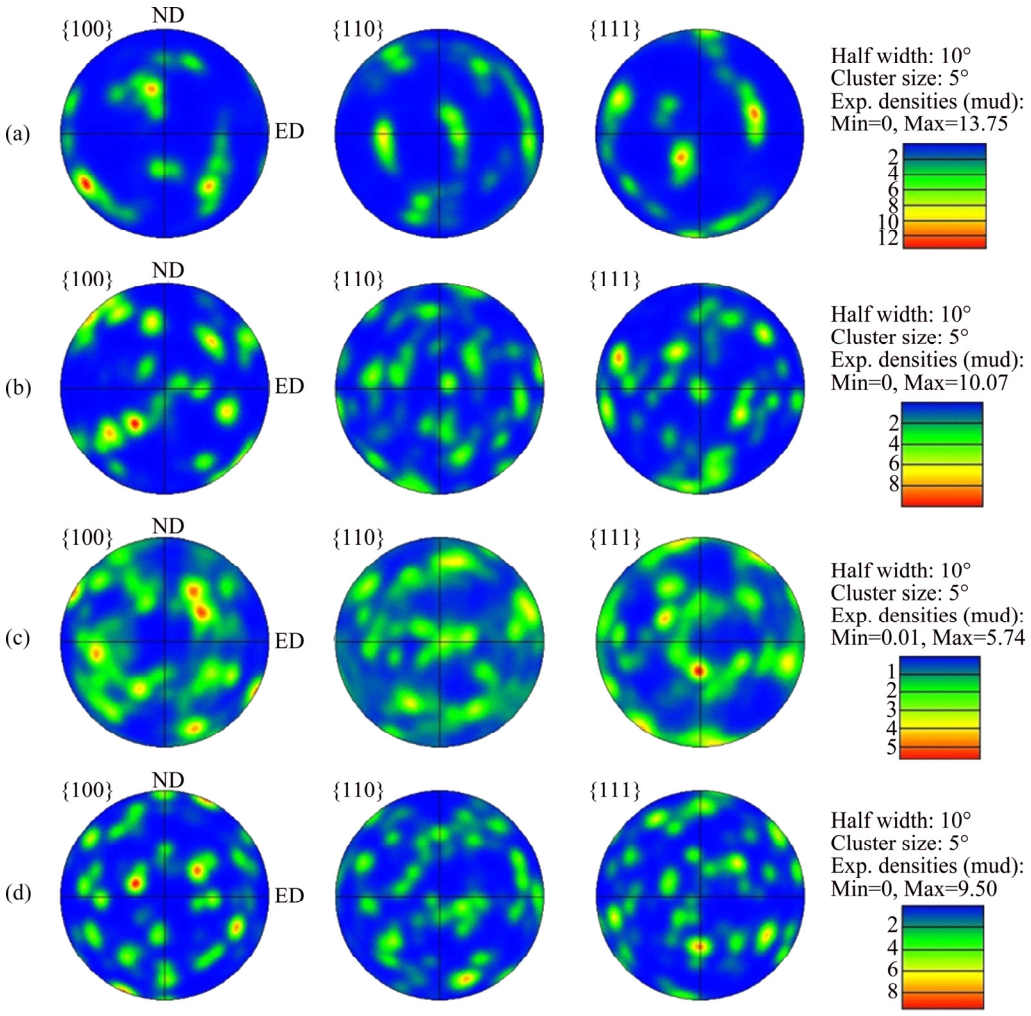

Fig. 19 Pole figures of ECREed 7005 alloy at various extrusion temperature (ND means *Z* direction and ED means *Y* direction): (a) 360 °C; (b) 380 °C; (c) 400 °C; (d) 420 °C

shown in Fig. 19, the texture intensity of ECREed 7005 alloy decreases obviously with the increase of extrusion temperature from 360 to 400 °C. When the extrusion temperature reaches 420 °C, the texture intensity increases again. The decrease of texture intensity with increasing extrusion temperature from 360 to 400 °C is attributed to the dynamic recovery and dynamic recrystallization in the ECRE process. The increase of texture intensity at 420 °C could be due to the fact that the interaction between the second phase and dislocation hinders the dynamic recovery and dynamic recrystallization. A decrease in the texture intensity also leads to a decrease of YS and UTS (Fig. 11). In addition, the (001) plane exhibits the strongest texture, and the (110) plane shows the weakest texture. The pole figure of 7075 alloy also showed (111) and (100) textures [41,42], but the texture intensity of one-pass and four-pass ECAEed 7075 alloy is smaller than that of this work.

Figure 20 shows bright field TEM images of the as-cast and ECREed 7005 alloys at various extrusion temperatures after T6 treatment. As shown in Fig. 20(a), there are still some obvious dislocations in the bright field image of TEM of the as-cast 7005 alloy. When the liquid 7005 alloy is poured into a metal mold, it solidifies quickly, leading to a non-equilibrium solidification process.

As a result, some dislocations are created in the as-cast 7005 alloy. Some dislocations remain in the as-cast 7005 alloy although relative dynamic recovery occurs in the T6 treatment. This could be due to the remained dislocations that lead to larger YS compared to the ECREed sample. When the 7005 alloy is processed by ECRE at 360 °C, some obvious long dislocations are noticed in the bright field image. It is attributed to relative dynamic recovery occurring in the ECRE process, leading to the orientation arrangement and the counteraction of dislocation. When the extrusion temperature is

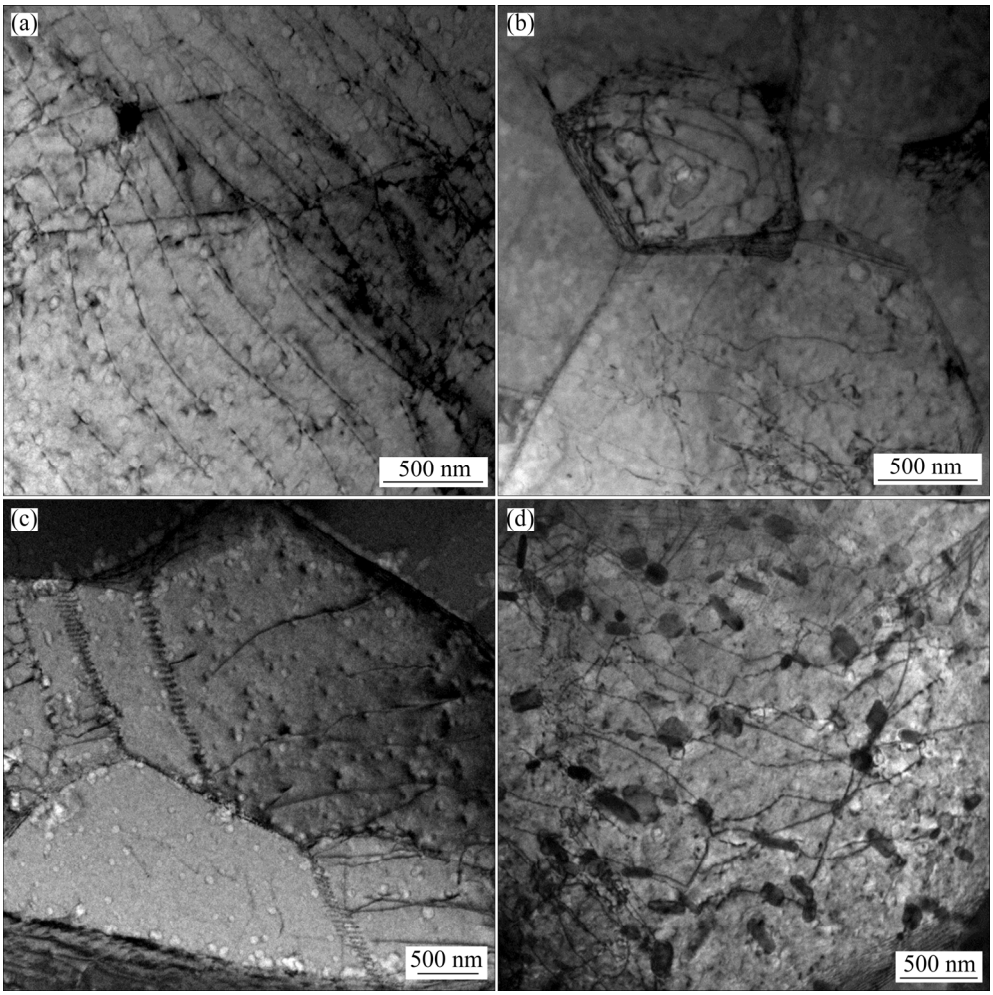

Fig. 20 Bright field TEM images of as-cast and ECREed 7005 alloys at various extrusion temperatures after T6 treatment: (a) 360 °C; (b) 380 °C; (c) 400 °C; (d) 420 °C

elevated to 380 and 400 °C, dynamically recrystallized grains are found in the TEM image (Figs. 20(b, c)). The size of the dynamically recrystallized grains varies from 0.9 to 2 μm. Dislocation density decreases obviously in the TEM image at 380 and 400 °C. However, there are still some dislocations in the dynamically recrystallized grains. This indicates that dislocation strengthening and fine-grain strengthening mechanisms play a role in improving the YS and UTS of the T6-treated ECREed sample together. Similar to TEM image of ECREed 7005 alloy without T6 treatment, interaction between the second phase and dislocation is noted in the TEM image of ECREed 7005 alloy after T6 treatment (Fig. 20(d)), which will improve the YS and UTS.

5 Conclusions

(1) Severe plastic deformation occurring in ECRE leads to a mixed microstructure including elongated grains, equiaxed grains and deformed dendrites instead of coarse dendrites of cast ingot. In addition, it also leads to an obvious improvement of the UTS and elongation of the deformed 7005 alloy via ECRE. Mechanical properties at Location 7 are higher than those at Location 6, because the material at Location 7 undergoes two ECAE deformation processes, but the material at Location 6 only undergoes one ECAE deformation process.

(2) Extrusion temperature has an important influence on mechanical properties of one-pass ECREed 7005 alloy. The YS and UTS decrease first and then increase with the increase of extrusion temperature from 360 to 420 °C. The highest YS of 288.9 MPa is obtained from the 7005 alloy ECREed at 360 °C, but the highest UTS of 441.2 MPa is achieved from the 7005 alloy ECREed at 420 °C. The elongation exhibits a peak value of 18.2% at 400 °C. The change of dislocation density and interaction between dislocation and the second phase lead to these phenomena.

(3) T6 treatment leads to an obvious improvement of mechanical properties of cast ingot and ECREed 7005 alloy. The YS of 359.2 MPa, UTS of 490 MPa and elongation of 17.7% are obtained after T6 treatment. The fine-grain strengthening, dislocation strengthening and precipitation strengthening together lead to a significant enhancement of mechanical properties. The fracture of ECREed 7005 alloy is characterized by a large number of small-size dimples, which also illustrates that good mechanical properties are obtained due to a ductile fracture. Brittle fracture gives an illustration of low elongation of cast ingot.

Acknowledgments

This work is supported by the National Natural Science Foundation of China (51875124).

References

[1] AGENA A S M. A study of flow characteristics of nanostructured Al-6082 alloy produced by ECAP under upsetting test [J]. Journal of Materials Processing Technology, 2009, 209: 856−863.

[2] CAO W Q, GODFREY A, LIU W, LIU Q. Annealing behavior of aluminium deformed by equal channel angular pressing [J]. Materials Letters, 2003, 57(24−25): 3767−3774.

[3] NAGASEKHAR A V, TICK-HON Y, SEOW H P. Deformation behavior and strain homogeneity in equal channel angular extrusion/pressing [J]. Journal of Materials Processing Technology, 2007, 192−193: 449−452.

[4] ABD EL ALL M I, SADAWY M M. Influence of ECAP as grain refinement technique on microstructure evolution, mechanical properties and corrosion behavior of pure aluminum [J]. Transactions of Nonferrous Metals Society of China, 2015, 25(12): 3865−3876.

[5] TOTH L S, GU C F. Ultrafine-grain metals by severe plastic deformation [J]. Materials Characterization, 2014, 92: 1−14.

[6] AGNEW S R, MEHROTRA P, LILLO T M, STOICA G M, LIAW P K. Crystallographic texture evolution of three wrought magnesium alloys during equal channel angular extrusion [J]. Materials Science and Engineering A, 2005, 408: 72−78.

[7] JIANG Ju-fu, WANG Ying, QU Jian-jun. Microstructure and mechanical properties of AZ61 alloys with large cross-sectional size fabricated by multi-pass ECAP [J]. Materials Science and Engineering A, 2013, 560: 473−480.

[8] AL-MAHARBI M, KARAMAN I, BEYERLEIN I J, FOLEY D, HARTWIG K T, KECSKES L J, MATHAUDHU S N. Microstructure, crystallographic texture, and plastic anisotropy evolution in an Mg alloy during equal channel angular extrusion processing [J]. Materials Science and Engineering A, 2011, 528: 7616−7627.

[9] LOBOS J, SUZUKI S, UTSUNOMIYA H, NAKAJIMA H, RODRIGEZ-PEREZ M A. Strengthening of lotus-type porous copper by ECAE process [J]. Journal of Materials Processing Technology, 2012, 212: 2007−2011.

[10] ETTER A L, BAUDIN T, REY C, PENELLE P. Microstructural and textural characterization of copper processed by ECAE [J]. Materials Characterization, 2006, 56: 19−25.

[11] KANG D H, KIM T W. Mechanical behavior and microstructural evolution of commercially pure titanium in enhanced multi-pass equal channel angular pressing and cold extrusion [J]. Materials & Design, 2010, 31(S1): s54−s60.

[12] SUWAS S, BEAUSIR B, TÓTH L S, FUNDENBERGER J J, GOTTSTEIN G. Texture evolution in commercially pure titanium after warm equal channel angular extrusion [J]. Acta Materialia, 2011, 59(3): 1121−1133.

[13] DEMIRTAS M, PURCEK G, YANAR H, ZHANG Z J, ZHANG Z F. Effect of equal-channel angular pressing on room temperature superplasticity of quasi-single phase Zn−0.3Al alloy [J]. Materials Science and Engineering A, 2015, 644: 17−24.

[14] XIANG Juan, HAN Yuan-fei, LI Jiu-xiao, QIU Pei-kun, SUN Xiang-long, LU Wei-jie, Microstructure characteristics of ECAP-processed (TiB+La_2O_3)/Ti−6Al−4V composites [J]. Journal of Alloys and Compounds, 2017, 726: 57−66.

[15] ANSARIAN I, SHAERI M H. Diffusional bonds in laminated composites produced by ECAP [J]. Transactions of Nonferrous Metals Society of China, 2017, 27(9): 1928−1938.

[16] PUERTAS I, PÉREZ C J L, SALCEDO D, LEÓN J, FUERTES J P, LURI R. Design and mechanical property analysis of AA1050 turbine blades manufactured by equal channel angular extrusion and isothermal forging [J]. Materials & Design, 2013, 52: 774−784.

[17] CHEGINI M, FALLAHI A, SHAERI M H. Effect of equal channel angular pressing (ECAP) on wear behavior of Al-7075 alloy [J]. Procedia Materials Science, 2015, 11: 95−100.

[18] LURI R, PÉREZ C J L, SALCEDO D, PUERTAS I, LEÓN J, PÉREZ I, FUERTES J P. Evolution of damage in AA-5083 processed by equal channel angular extrusion using different die geometries [J]. Journal of Materials Processing Technology, 2011, 211: 48−56.

[19] NIKULIN I, KAIBYSHEV R, SAKAI T. Superplasticity in a 7055 aluminum alloy processed by ECAE and subsequent isothermal rolling [J]. Materials Science and Engineering A, 2005, 407: 62−70.

[20] STOLYAROV V V, LAPOVOK R, BRODOVA I G, THOMSON P F. Ultrafine-grained Al–5wt.%Fe alloy processed by ECAP with backpressure [J]. Materials Science and Engineering A, 2003, 357: 159−167.

[21] LANGDON T G. Twenty-five years of ultrafine-grained materials: Achieving exceptional properties through grain refinement [J]. Acta Materialia, 2013, 61(19): 7035−7059.

[22] VALIEV R Z, LANGDON T G. Principles of equal-channel angular pressing as a processing tool for grain refinement [J]. Progress in Materials Science, 2006, 51(7): 881−981.

[23] BEYERLEIN I J, TÓTH L S. Texture evolution in equal-channel angular extrusion [J]. Progress in Materials Science, 2009, 54(4): 427−510.

[24] JIANG Ju-fu, LUO Shou-jing. Reheating microstructure of refined AZ91D magnesium alloy in semi-solid state [J]. Transactions of Nonferrous Metals Society of China, 2004, 14(6): 1074−1081.

[25] JIANG Ju-fu, WANG Ying, LUO Shou-jing. Application of equal channel angular extrusion to semi-solid processing of magnesium alloy [J]. Materials Characterization, 2007, 58: 190−196.

[26] JIANG Ju-fu, LUO Shou-jing. Microstructure evolution of AZ91D magnesium alloy semi-solid billets prepared by a new SIMA method [J]. Solid State Phenomena, 2006, 116−117: 132−135.

[27] JIANG Ju-fu, LIN Xin, WANG Ying, QU Jian-jun, LUO Shou-jing. Microstructural evolution of AZ61 magnesium alloy predeformed by ECAE during semisolid isothermal treatment [J]. Transactions of Nonferrous Metals Society of China, 2012, 22(3): 555−563.

[28] JIANG Ju-fu, WANG Ying, DU Zhi-ming, LUO Shou-jing. Microstructure and properties of AZ80 alloy semisolid billets fabricated by new strain induced melt activated method [J]. Transactions of Nonferrous Metals Society of China, 2012, 22(S2): s422−s427.

[29] JIANG Ju-fu, WANG Ying, QU Jian-jun, DU Zhi-ming, SUN Yi, LUO Shou-jing. Microstructure evolution of AM60 magnesium alloy semisolid slurry prepared by new SIMA [J]. Journal of Alloys and Compounds, 2010, 497: 62−67.

[30] ZHAO Zu-de, CHEN Qiang, WANG Yan-bin, SHU Da-yu. Microstructural evolution of an ECAE-formed ZK60-RE magnesium alloy in the semi-solid state [J]. Materials Science and Engineering A, 2009, 506: 8−15.

[31] DAMAVANDI E, NOUROUZI S, RABIEE S M, JAMAATI R. Effect of ECAP on microstructure and tensile properties of A390 aluminum alloy [J]. Transactions of Nonferrous Metals Society of China, 2019, 29(5): 931−940.

[32] MESHKABADI R, FARAJI G, JAVDANI A, POUYAFAR V. Combined effects of ECAP and subsequent heating parameters on semi-solid microstructure of 7075 aluminum alloy [J]. Transactions of Nonferrous Metals Society of China, 2016, 26(12): 3091−3101.

[33] PRONI C T W, TORRES L V, HAGHAYEGHI R, ZOQUI E J. ECAP: An Alternative route for producing AlSiCu for use in SSM processing [J]. Materials Characterization, 2016, 118: 252−262.

[34] ASHOURI S, NILI-AHMADABADI M, MORADI M, IRANPOUR M. Semi-solid microstructure evolution during reheating of aluminum A356 alloy deformed severely by ECAP [J]. Journal of Alloys and Compounds, 2008, 466: 67−72.

[35] SPUSKANYUK V, SPUSKANYUK A, VARYUKHIN V. Development of the equal-channel angular hydroextrusion [J]. Journal of Materials Processing Technology, 2008, 203: 305−309.

[36] GB 6397—86. Metal tensile test specimens [S].

[37] HUANG K, LOGÉ R E. A review of dynamic recrystallization phenomena in metallic materials [J]. Materials & Design, 2016, 111(5): 548−574.

[38] FLEMINGS M C. Behavior of metal alloys in the semisolid state [J]. Metallurgical Transactions B, 1991, 22: 269−293.

[39] IWAHASHI Y, WANG J, HORITA Z, NEMOTO M, LANGDON T G. Principle of equal-channel angular pressing for the processing of ultra-fine grained materials [J]. Scripta Materialia, 1996, 35(2): 143−146.

[40] RAAB G J, VALIEV R Z, LOWE T C, ZHU Y T. Continuous processing of ultrafine grained Al by ECAP−Conform [J]. Materials Science and Engineering A, 2004, 382: 30−34.

[41] SHAERI M H, SALEHI M T, SEYYEDEIN S H, ABUTALEBI M R, PARK J K. Characterization of microstructure and deformation texture during equal channel Angular pressing of Al−Zn−Mg−Cu alloy [J]. Journal of

Alloys and Compounds, 2013, 576: 350−357.
[42] SHAERI M H, SHAERI M, SALEHI M T, SEYYEDEIN S H, DJAVANROODI F. Microstructure and texture evolution of Al 7075 alloy processed by equal channel angular pressing [J]. Transactions of Nonferrous Metals Society of China, 2015, 25(5): 1367−1375.

单道次等通道往复挤压变形 7005 铝合金的显微组织与力学性能

姜巨福[1]，王 迎[2]，刘英泽[1]，肖冠菲[1]，李 华[2]

1. 哈尔滨工业大学 材料科学与工程学院，哈尔滨 150001；
2. 哈尔滨工业大学 机电工程工程学院，哈尔滨 150001

摘 要：首次提出等通道往复挤压技术，用于 7005 铝合金以获得大塑性变形。研究单道次等通道往复挤压变形 7005 铝合金的显微组织和力学性能。结果表明，在等通道往复挤压中发生的大塑性变形导致变形材料由混晶组织组成。等通道往复挤压变形的 7005 铝合金呈现抗拉强度和伸长率的大幅提升。在经历完整的等通道往复挤压过程的区域，材料的力学性能比其他区域的力学性能高，这主要由于材料可获得更大的位错强化。屈服强度和抗拉强度随着挤压温度的升高呈现先增加后降低的趋势。当等通道往复挤压的 7005 铝合金经过 T6 热处理后，其屈服强度为 359.2 MPa，抗拉强度为 490 MPa，伸长率为 17.7%。细晶强化、位错强化和析出相强化共同在提升热处理后材料力学性能方面起着重要作用。

关键词：7005 铝合金；等通道往复挤压；显微组织；力学性能

(Edited by Bing YANG)